Imaging Tools for Evaluation of Gusset Plate Connections in Steel Truss Bridges

by

Christopher Higgins[1] and O. Tugrul Turan[2]

Abstract

After the collapse of the I35W Bridge in Minneapolis, MN in 2007, transportation agencies began evaluating and rating their inventories of gusset plate connections. Connection evaluations require accurate drawings that detail the plate, member, and fastener geometries. These structural details should also accurately reflect the as-built conditions. For some connections, as-built information may not be available or the available drawings may not represent the actual field conditions. To fill this gap, a new methodology was developed that enables rapid and accurate collection of field measurements for connection plate geometry. The method uses close-range photogrammetry techniques to rectify images taken with consumer grade cameras using flat-field and fisheye lenses. The technique has been demonstrated on full-scale gusset plates in the laboratory and in the field. Dimensional measurements from the processed images provided results that are as good as or better than conventional field measurements and with tolerances below what most engineers require for calculation of gusset plate connection capacity. This technique provides a new tool for bridge engineers to quickly collect gusset plate geometry that can be used in connection evaluations and rating, and can further enhance bridge management tasks.

[1] Professor and Slayden Construction Faculty Fellow, [2] Post-Doctoral Research Associate, School of Civil and Const. Engineering, Oregon State University, Corvallis, OR 97331

Introduction and Background

After the collapse of the I-35W Bridge in Minneapolis, MN in 2007, gusset plate connections have become a focus of transportation agencies. Several approaches have been developed to aid engineers in evaluation of gusset plates including the Federal Highway Administration (FHWA) (2009) load rating guideline; finite element analyses of gusset plates in the I-35W Bridge (Hao 2010 and Minmao *et al.*, 2010); expected rating factor formulas considering block-shear and Whitmore sections (Higgins *et al.* 2010a); simple and rapid ranking methods to identify likely vulnerable gusset plates (Higgins *et al.* 2010b); and a procedure to eliminate detailed checking of gusset plates that have adequate capacity (Berman *et al.* 2011).

Regardless of the approach considered, connection evaluations and analyses require accurate geometric data of the gusset plate as inputs. Current methods used to measure, collect, and archive field geometric data are time consuming, expensive, and are subject to errors. This is especially true for finite element analyses where all the fastener locations and dimensions of the gusset plate must be established. For this level of detail, sketches, notes, and qualitative photographs do not provide sufficient fidelity to accurately characterize connection geometry. New techniques are needed to effectively capture field data to hasten the complex and time consuming task of steel truss bridge connection evaluation.

Visual inspection methods are now beginning to deploy supporting technologies that can improve and accelerate structural evaluations (McCrea *et al.* 2002). One type of technology is digital image processing, which has been utilized in various civil engineering fields. Several researchers implemented digital image technologies for assessment and inspection of steel, concrete and reinforced concrete structures. Although using digital image processing to detect a crack on a concrete surface is difficult due to voids, blemishes, shading, and shapes of cracks, it has attracted broad interest and been studied by several researches such as Ito *et al.* (2002), Dare *et al.* (2002), Hutchinson and Chen (2006), Fujita *et al.* (2006), Yamaguchi and Hashimoto (2006), Sinha and Fieguth (2006), Yamaguchi *et al.* (2008), and Yamaguchi and Hashimoto (2009). Lee and Chang

(2005) used digital image processing for the assessment of rust defects on steel bridges. Liu *et al.* (2006) utilized image processing methods to detect rivets for aircraft lap joints. In this paper digital image processing is used to rectify digital photographs to produce scaled orthographic images (orthophotos) of steel truss bridge gusset plate connections so that physical dimensions can be extracted and used in connection evaluation.

Image Rectification and Metrification with Flat-Field Lenses

Simple and effective close-range photogrammetry techniques have been utilized in historical building documentation (Arias *et al.*, 2007) and several researchers have used close-range photogrammetry for metrification such as Heuvel (1998), Criminisi (2000), Tommaselli *et al*. (2005), Rodriguez *et al.* (2008). The present study is different from previous work because images of bridge connections cannot easily be taken from stationary points. For practical applications, images of bridge gusset plates are taken from a snooper or using climbing techniques where both the camera and bridge are moving due to wind and traffic, thus it is impractical to use stationary positions to correlate stereo or multi-station images.

Photographic images are collected of a real world scene and placed on a two-dimensional image plane. When an image is captured with a camera and lens, it generally contains perspective distortion (parallel lines converging at a finite point), as well as other distortions due to the lens characteristics (typically radial aberrations). To remove perspective, the image can be rectified using a mathematical transformation which relates the real world image to that on the photographic image plane. Removal of radial distortion for some lenses requires lens correction parameters applied during post-processing of the images. Alternatively, and as implemented in the present work, flat-field lenses that do not have these aberrations are deployed.

When the real world features correspond to a single plane, as is the case for most gusset plate connections, two-dimensional correspondences are used to rectify the image. This simplifies the transformation. The most common technique used for image rectification is the direct linear transformation (DLT) algorithm. This transformation requires that

geometrical characteristics be established between in the real world image and the image plane. In the present work, point correspondences are used to map points between the real world image and the photographic image plane based on central projection. Central projection maps the common points between planes and preserves straight lines in both planes.

It is possible to establish the geometrical features to provide a true dimensional scale such that the resulting transformation is not only rectified; it is scaled to the real world dimensions. This enables measurements to be taken from the rectified image, as pixels are transformed into units of dimension. Implementation of the DLT algorithm assumes that the image plane and real world planes are homogeneous. A transformation matrix, H, is determined to satisfy the following equation for each control point, i:

$$H\begin{bmatrix} x_i' \\ y_i' \\ 1 \end{bmatrix} = \begin{bmatrix} x_i \\ y_i \\ 1 \end{bmatrix} \tag{1}$$

where x_i' and y_i' are photograph image plane control point coordinates, x_i and y_i are real world control point coordinates. The transformation matrix H is a 3x3 matrix. To determine the transformation matrix, control points of known location must be established in the real world image. These are then captured on the image plane. A minimum of four control points are needed (x and y coordinates each provide a degree-of freedom (DOF) for a total of eight DOFs and one more is provided by scale, thereby providing nine DOFs to solve for the matrix). The method generates a two-dimensional transformation based solely on the control point coordinates. Thus, camera calibration is not needed.

In the present work, a reference target was developed that establishes the relation between the real world control points and the image control points. The target has nine control points, which are more than needed to define the transformation matrix. The arms

of the target are 609.6 mm (24 in.) long and consist of 12.7 mm (0.5 in.) square Ultra Corrosion-Resistant Pure Titanium Grade 2 bars, nine aluminum discs that serve as the control points, and a steel encased round ceramic magnet. The titanium bars are placed in a cruciform shape as shown in Fig.1. Ideally, these control points are spread throughout the image.

Since the reference target control points standoff from the surface of the gusset plate to enable clearance over bolt and rivet heads, the standoff distance causes the reference target points to appear larger in the photograph than if they were on the gusset plate surface. The offset is corrected assuming the camera is a single point and using similar triangles to calculate the apparent size increase of the reference target. The standoff distance for the reference target is 50.8 mm (2 in.) from the gusset plate surface. The actual lengths of the gusset plate features including the offset correction can be calculated as:

$$L_{actual} = \frac{D}{D - D_o} L_{image} \tag{2}$$

where D is the distance from the camera to the gusset plate surface, D_o is the standoff distance, and L_{image} is the uncorrected length measured in the rectified image. Dimensions taken from the rectified image without standoff correction will be smaller than the true dimensions. If the camera location is far away from the target, the correction becomes small (for example correction is less than 5% for camera located 1.5 m (5 ft) from the gusset plate). Alternatively, a known distance can be marked on the gusset place surface as a reference and that distance can be used as a scale for metrification.

The image rectification and metrification process was written using MATLAB (The Mathworks, 2010) and deploys the Image Processing Toolbox within MATLAB. A digital image of a gusset plate with the reference target is taken. The gusset plate digital photograph is loaded into the program and the image pixels of the reference targets are selected by the user. These establish the known real world target coordinates for the DLT algorithm. As part of the processing, an origin is established at the center of the target. The rectified image is presented to the user for validation and then stored for future

reference. After processing, the user can query the image to extract geometric data of interest, because the methodology has converted the pixel size to a true-scale dimension (for example - inch).

To illustrate the methodology and find the difference between measured and the computer numerical control machine (CNC) fabricated gusset plate dimensions, a full size CNC fabricated gusset plate was used. Images were captured with a digital single-lens reflex (SLR) camera made by Nikon (Nikon D300s). The camera uses a 12.3 Megapixel (4288 x 2848) CMOS sensor. The lens was an autofocus fixed 60 mm f2.8D lens. The non-metric digital camera was not calibrated. Field inspectors will likely be using a variety of digital cameras with various lenses and zoom capability and these cameras will not be mounted on a tripod or stationary platform while images are taken. Controlled calibration may not be feasible or transferable to field applications and thus, cameras and the techniques deployed must be compatible with hand-held operation under realistic field conditions. To reflect these conditions, the images were taken in the laboratory under realistic imaging conditions. Three images; 90 degrees between the gusset plate surface and the normal of the image plane (S90), 30 degrees between the gusset plate surface and the normal of the image plane from the left (S30L), 30 degrees between the gusset plate surface and the normal of the image plane from right (S30R), were taken. The original and rectified images are shown in Fig. 2. Qualitative comparison of the collected geometry of the gusset plate and the original geometry are shown in Fig.3.

In order to conduct a quantitative comparison with respect to the present application to gusset plate evaluation, the procedures in the FHWA Load Rating Guidance and Examples for Bolted and Riveted Gusset Plates in Truss Bridges (FHWA, 2009) were used. To perform evaluations of the various connection failure modes, input geometries are needed. Geometric measures for the following modes were used: gross length along the plane resisting tension stress Bl. Sh. (T) and gross length along the plane resisting shear stress (Bl. Sh. (V)) for block shear evaluation of every member in the gusset plate, unbraced buckling length (Buc. Len.) and Whitmore Width (W. Width) and for every

compression member, gross length of the plate resisting horizontal shear (H. Sh.), gross length of the plate resisting vertical shear (H. Sh.) and edge lengths (A, B, C, D, E, F) were measured as shown in Fig. 4. Results are tabulated in Table 1. Since the measurements are sometimes more than the original and vice versa, the absolute value of the maximum is reported. The observed maximum differences were 0.92%, 1.91% and 1.86%; and the mean differences were -0.07%, 0.12% and 0.18% for S90, S30L and S30R, respectively. As expected, the image with the least amount of initial perspective, S90, produced slightly better results. However, even the other two images with strong perspective provided quite good outcomes that are well within the expected needs of bridge engineers performing connection evaluations.

Image Stitching, Rectification and Metrification with Flat-Field Lenses

Sometimes it is not possible to capture an entire gusset plate and its fasteners in a single image as shown in Fig 5a, where an obstruction obscures the plate. In this case, multiple images of the gusset plate are taken and these can be assembled to produce a single composite image. To do this, and retain the metrification quality of the images, an image stitching program was created using MATLAB (The Mathworks, 2010).

In order to stitch two images together, one of the images (Image 1), Fig. 5a, is selected as the base image and the other one (Image 2), Fig. 5b, is selected as the image that needs to be transformed to integrate with the base image (Image 1). In order to transform Image 2, points of correspondence between the two images are used to create a transformation matrix that is applied to Image 2. Projective transformation (Straight lines remain straight, however parallel lines converge toward vanishing points) (Matlab 2010b, Mathworks) was used in the program and for this type of transformation at least four points are needed and the images may or may not be rectified before stitching. After creating the transformation matrix, the stitched image size is calculated. Since three channel RGB (red, green and blue) images were used, two black arrays with the same size as the (RGB=0, 0, 0) images were created and the base image and the transformed images are pasted onto these black arrays. The transformed image is subtracted from the base image and the subtracted image is obtained. The subtracted image is added to the

transformed image and the composite stitched image is obtained as shown in Fig. 5c. The procedure for adding and subtracting image pieces is summarized in Fig. 6.

If obstructions occur in the composite image, these can be removed in the final image. Using a closed polygon defined by the user, the pixels can be replaced by either the base image or/and transformed image as shown in Fig 5d.

Using the geometric parameters described in the previous section for single images, a quantitative comparison was conducted using the combined final image (Sti.). Results are tabulated in Table 1. The observed maximum and mean differences were 1.51%, and -0.21%, respectively.

Using all of the flat-field lens image measurements (S90, S30L, S30R and Sti.), a histogram was created and is shown in Fig. 7a. The standard deviation was 0.61%, skewness was -0.24%, the mean was 0.00%, and there was a 99% probability that a measurement was within +/- 1.6% of the actual.

Image Rectification and Metrification with Fisheye Lenses

Flat-field lenses were used in the previous development in order to minimize the effect of barrel distortion and/or pin-cushion. However, due to the size and short available standoff distance, it is sometimes difficult to capture the whole gusset plate in one picture with a short focal length lens. Furthermore, sometimes due to obstacles such as another gusset plate, floor beam, lateral bracing, utility pipe etc., as shown in Fig.8a; it is impossible to capture the whole gusset plate in one picture with a flat-field lens. For these cases, a fisheye lens can be utilized to capture a large part of the structure with short focal lengths as shown in Fig.8b. This fisheye image can then be converted to a perspective image (defish), shown in Fig. 8c, so that the converted image (defished image) can be used in rectification and metrification procedures as described above.

Fisheye lenses are lenses that can provide a wide field of view with a very short focal length. These lenses can be used to capture 180^{o} or larger field of view with a single

camera, from one stationary point and at a single moment (Abraham and Forstner, 2005). Compared to a true panoramic cameras, they are cheap and can be combined with conventional cameras (Scheneider *et al.*, 2009).

In fisheye projection models, generally a sphere is projected on a plane and depending on their projection geometry; they can be classified in four different categories: Equidistant Projection, Equisolid-angle Projection, Othographic Projection and Stereographic Projection (Ray, 1994). Most of fisheye lenses are either Equisolid-angle Projection or Equidistant Projection. In this paper Equisolid-angle Projection was used for defishing images.

In perspective projection, an object in space can be described in the camera coordinate system as (x, y, z) and the same object can be described in the image coordinate system as $(x_1^{'}, y_1^{'})$ where x and y axes and $x_1^{'}$ and $y_1^{'}$ axes are parallel. Using this notation, the incidence angle, α, image radius, r' and the mapping function of an undistorted perspective image can be written (Scheneider *et al.*, 2009) as:

$$\tan(\alpha) = \frac{\sqrt{x^2 + y^2}}{z} \tag{3}$$

$$r' = \sqrt{x'^2 + y'^2} \tag{4}$$

$$r' = c_1 \tan(\alpha) \tag{5}$$

$$\frac{x_1^{'}}{y_1^{'}} = \frac{x}{y} \tag{6}$$

where c_1 is the principle distance of the undistorted perspective image. Using Eqs.5-6 $(x_1^{'}, y_1^{'})$ can be written as:

$$\begin{aligned} x_1^{'} &= \frac{r'}{\sqrt{\left(\frac{y}{x}\right)^2 + 1}} \\ y_1^{'} &= \frac{r'}{\sqrt{\left(\frac{x}{y}\right)^2 + 1}} \end{aligned} \tag{7}$$

Utilizing Eq.3, 5; $(x_1^{'}, y_1^{'})$ can also be written as:

$$x_1^{'} = \frac{c_1 \frac{\sqrt{x^2 + y^2}}{z}}{\sqrt{\left(\frac{y}{x}\right)^2 + 1}}$$
$$y_1^{'} = \frac{c_1 \frac{\sqrt{x^2 + y^2}}{z}}{\sqrt{\left(\frac{x}{y}\right)^2 + 1}} \quad (8)$$

For the undistorted fisheye projection models, the mapping functions and the projection equation for Equisolid-angle Projection can be written (with correction parameters ignored) (Scheneider *et al*, 2009) as:

$$r' = 2c_2 \sin(\frac{\alpha}{2}) \quad (9)$$

$$x_2^{'} = 2c_2 \frac{\sin(\frac{1}{2}\arctan(\frac{\sqrt{x^2 + y^2}}{z}))}{\sqrt{\left(\frac{y}{x}\right)^2 + 1}}$$
$$y_2^{'} = 2c_2 \frac{\sin(\frac{1}{2}\arctan(\frac{\sqrt{x^2 + y^2}}{z}))}{\sqrt{\left(\frac{x}{y}\right)^2 + 1}} \quad (10)$$

In order to convert fisheye images to perspective images, fisheye images are assumed to be undistorted (correction parameters are ignored). For Equisolid-angle Projection, the perspective image coordinates were derived for the fisheye projection equations by mapping to the real world image coordinates using Eqs. 8-10 as:

$$x_1^{'} = c_1 \frac{\tan(2\sin^{-1}(\frac{x_2^{'}}{2c_2}\sqrt{\left(\frac{y_2^{'}}{x_2^{'}}\right)^2+1}))}{\sqrt{\left(\frac{y_2^{'}}{x_2^{'}}\right)^2+1}}$$
$$y_1^{'} = c_1 \frac{\tan(2\sin^{-1}(\frac{y_2^{'}}{2c_2}\sqrt{\left(\frac{x_2^{'}}{y_2^{'}}\right)^2+1}))}{\sqrt{\left(\frac{x_2^{'}}{y_2^{'}}\right)^2+1}} \quad (11)$$

Using Eq. 11, a Matlab image processing program was written. Three images; 61 cm (2 ft) away from the gusset plate (F2ft), 91 cm (3 ft) away from the gusset plate (F3ft), and 152.4 cm (5 ft) away from the gusset plate (F5ft); were taken with a Nikkor 10.5 mm lens which uses Equisolid-angle Projection. The principle distance in the x (c_{2X}) and y (c_{2Y}) directions are calculated as 1918.70 pixels (the maximum resolution in the x direction (4288) divided by the sensor size in the x direction (23.6 mm) and multiplied by the focal length (10.56 mm)) and 1903.44 pixels (the maximum resolution in the y direction (2848) is divided by the sensor size in the y direction (15.8 mm) and multiplied by the focal length (10.56 mm)). The principle distance of the perspective image (c_1) was 600 pixels which provided a large field of view from the fisheye images used in this paper. Larger values would produce a smaller portion of the image but with larger numbers of pixels across the image. The value can be selected interactively to focus on the essential part of the image and disregard superfluous portions.

The program first creates an array with the same size of the input image (fisheye image) with zeros (black) placed into the three channels (RGB (red, green, and blue). For every pixel location in the defished image, using Eq. 11 and the principle distances; the corresponding pixel location in the fisheye image was calculated. The RGB values in the fisheye image location were copied to the defished image location. If the defished image location was out of the fisheye image index, then that pixel was left blank (black). Thus, for every defished image location pixel values, the fisheye image location pixel values are copied and the defished image is created. Results are shown in Fig. 9.

Using the geometric parameters and the rectification technique described above, a quantitative comparison was conducted for each of the structural evaluation parameters described in the earlier section. Since the pictures are taken with fisheye lenses, standoff correction was not used in the metrification. Measured distances were marked on the gusset plate surface and these distances were used as a scale for metrification. Results are tabulated in Table 2. The observed maximum differences were 1.83%, 1.56% and 1.11%; and the observed mean differences were 0.16%, 0.10% and 0.11% for F2ft, F3ft and F5ft, respectively. The results from the fisheye lens were not quite as good as those observed for flat-field lenses, but are still quite acceptable for engineering evaluations. Using all the fisheye image measurements, a histogram was created and is shown in Fig. 7b. The standard deviation was 0.67%, skewness was 0.33%, the mean was 0.12% , and there was a 99% probability that an image measurement was within +/- 1.7% of the actual. These results were comparable to the flat-field lens demonstrated previously.

Conclusions

An innovative methodology that enables rectification and metrification of digital images of steel truss gusset plate connections was developed. Three different programs were developed that enable an operator to quickly extract dimensional information from the scaled rectified images. Flat and fisheye lenses were used and compared with the original dimensions of a large field-scale gusset plate. The largest of the absolute maximum and mean differences between the measured and expected dimensions were 1.91% and 0.21% respectively. Dimensional measurements taken from the processed images provided results that are as good as or better than conventional field measurements and provide tolerances well below what most engineers would accept for gusset plate connection capacity calculations. Compared to traditional methods, the current method enables much more rapid, accurate, and repeatable collection of field geometric measurements. The availability of rectified pictures with metric information provides a useful record of field conditions that can be referenced in the future and compared with subsequent field inspection results to help identify and quantify long term changes in visual characteristics. These images enable comparison between available drawing sets and as-

built details. Furthermore, they can be used to develop input geometries for finite element analyses of gusset plates or production of computer aided design drawings. The implementation procedure is straightforward and does not require any specialized knowledge of photogrammetry, image processing, or programming. It has been practically employed under field conditions using current technology and personnel.

Acknowledgements

This research was funded by the Oregon Department of Transportation. The input and support of Messrs. Bert Hartman, Jonathan Rooper, Jeff Swanstrom, Richard Groff, and Steven Soltesz was greatly appreciated. Mr. Quang Nguyen and Mr. Jason Killian of Oregon State University provided assistance during early development of the image processing algorithms. The findings, conclusions, and recommendations presented are those of the authors and do not necessarily reflect the views of the project sponsors or individuals acknowledged.

REFERENCES

Abraham, S., Forstner, W., (2005) "Fish-eye-stereo calibration and epipolar rectification" ISPRS Journal of Photogrammetry and Remote Sensing, v. 59, n. 5, 278-288.

Arias, P., C. Ordóñez, H. Lorenzo, J. Herraez, and J. Armesto., (2007) "Low-cost documentation of traditional agro-industrial buildings by close-range photogrammetry", Building and Environment, 42: 1817-1827.

Berman J. W., Wang, B., Olson, A. W., Roeder, C.W., Lehman, D. E., (2011) "Rapid assessment of gusset plate safety in steel truss bridges" ASCE Journal of Bridge Engineering, (in preview: http://dx.doi.org/10.1061/(ASCE)BE.1943-5592.0000246)

Criminisi, A., I. Reid, and A. Zisserman., (2000) "Single view metrology", Int. J. of Comp. Vision, 40: 123-148.

Dare, P. M., Hanley, H. B., Fraser, C. S., Riedel, B., Niemeier, W., (2002) "An operational application of automatic feature extraction: the measurement of cracks in concrete structures", The Photogrammetric Record, 17 (99), 453-464.

FHWA (2009). Load rating guidance and examples for bolted and riveted gusset plates in truss bridges" Publication No. FHWA-IF-09-014, Federal Highway Administration.

Fujita, Y., Mitane, Y., Hamamoto, Y., (2006), "A method for crack detection on a concrete structure", The 18th International Conference on Pattern Recognition.

Hao, S. (2010) "I-35 bridge collapse" ASCE Journal of Bridge Engineering, vol.15, no.5, pp 608-614.

Heuvel, F., (1998) "3D reconstruction from a single image using geometric constraints", ISPRS J. of Photogrammetry and Remote Sensing, 53: 354-368. (1998).

Higgins, C., Turan, O.T., and Connor R.J. (2010a) "Rapid ranking procedures for gusset plate connections in existing steel truss bridges" ASCE Journal of Bridge Engineering, vol.15, no.5, pp 581-596

Higgins, C., Senturk, A.E., and Turan, O.T. (2010b) "Comparison of block-shear and Whitmore Section methods for load rating existing steel truss gusset plate connections" ASCE Journal of Bridge Engineering, vol. 15, no. 2, pp 160-171.

Hutchinson, T. C., Chen, Z., (2006), "Improved image analysis for evaluation concrete damage", Journal of Computing in Civil Engineering 20 (3), 210-216.

Ito, A., Aoki, Y., Hashimoto, S., (2002). " Accurate extraction and measurement of fine cracks from concrete block surface image." 3, 2202-2207.

Liu, Z., Forsyth, D. S., Marincak, A., Vesley, P., (2006). " Automated rivet detection in the EOL image for aircraft lap joints inspection." NDT&E International, 39, 441-448.

Lee, S., Chang, L., (2005). "Digital image processing methods for assessing bridge painting rust defects and their limitations."ASCE International Conference on Computing in Civil Engineering.

Matlab 7.11.0 (R2010b), (2010) The MathWorks, Inc., Natick, MA.

McCrea, A., Chamberlain, D., Navon, R., (2002). "Automated inspection and restoration of steel bridges-a critical review of methods and enabling technologies." Automation in Construction, 11 (4), 351-373.

Minmao L., Okazaki, T., Roberto, B., Schultz, A.E., and Galambos, T.V. (2010) "Nonlinear finite-element analysis of critical gusset plates in the I-35W bridge in Minnesota" ASCE Journal of Structural Engineering vol. 137, no 1, pp 59-68.

Parr, M. J., Connor, R. J., and Bowman, M. (2010) "Proposed method for determining the interval for hands-on inspection of steel bridges with fracture critical members" ASCE Journal of Bridge Engineering, vol. 15, no. 4, pp 352-363.

Ray, S. F., (2002). "Applied photographic optics: lenses and optical systems for photography, film, video, electronic and digital imaging, Third Edition, Focal Press.

Rodríguez, J., M.T. Martín, P. Arias, C. Ordóñez, and J. Herráez. (2008) “Flat elements on buildings using close-range photogrammetry and laser distance measurement”, Optics and Lasers in Engineering, 46: 541-545.

Schneider, D., Schwalbe, E., Maas, H. G. (2009) “Validation of geometric models for fisheye lenses” ISPRS Journal of Photogrammetry and Remote Sensing, v. 64, n. 3, 259-266

Tommaselli, A. and M. Reiss., (2005) “A photogrammetric method for single image orientation and measurement, Photogrammetric Engineering and Remote Sensing”, 71(6): 727-732.

Yamaguchi T., Hashimoto, S., (2006), “Automated crack detection for concrete surface image using percolation model and edge information” Proceedings of the 32nd Annual Conference of the IEEE Industrial Electronics Society.

Yamaguchi, T., Nakamura, S., Hashimoto, S., (2008), “An efficient crack detection method using percolation-based image processing.” Proceedings of the 3rd IEEE Conference on Industrial Electronics and Applications.

Yamaguchi, T., Hashimoto, S., (2009), “Fast crack detection method for large size concrete surface images using percolation based image processing” Machine Vision and Applications 21, (5), 797-809.

Figures:

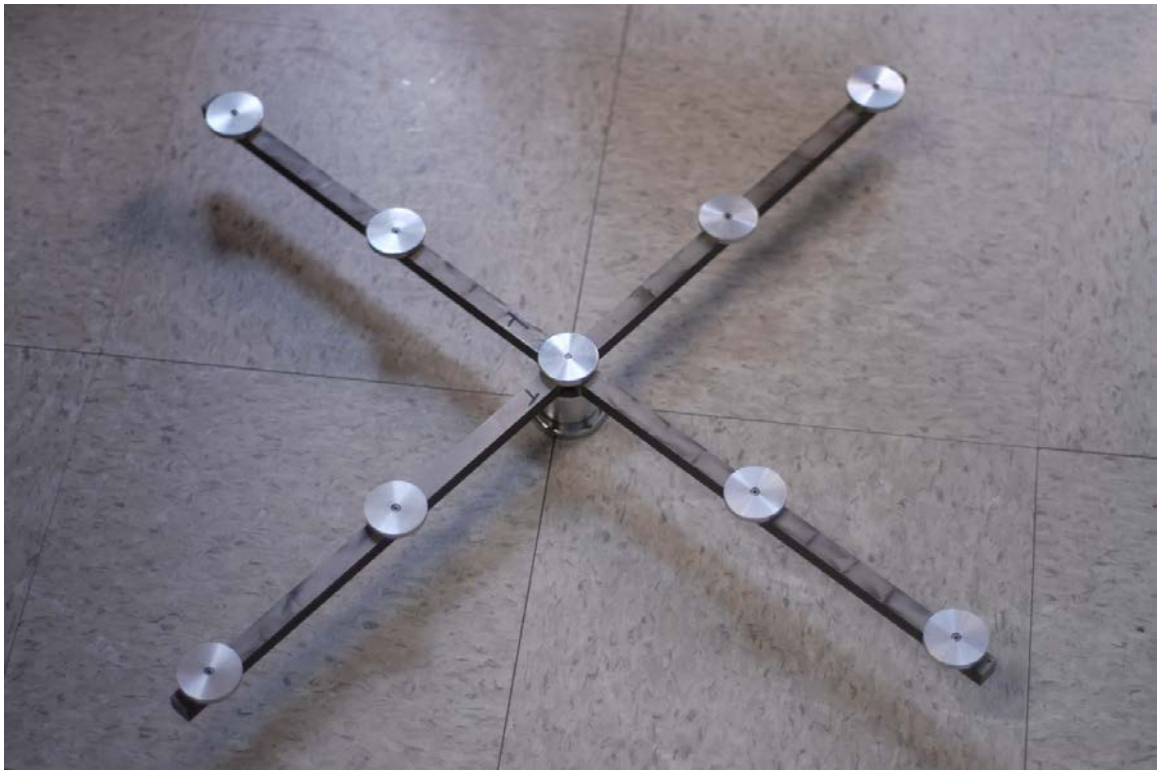

Fig. 1. Reference target used to establish nine (9) control points in real world image.

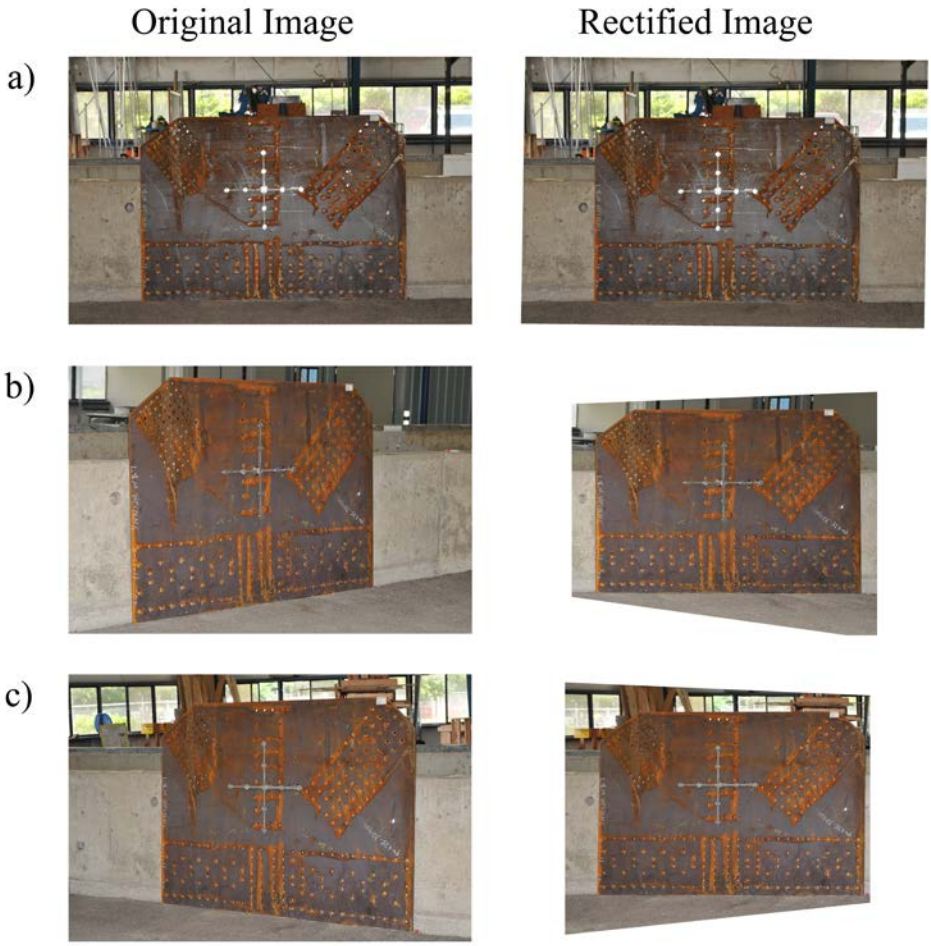

Fig. 2. Original and rectified images a) S90, b) S30L and c) S30R

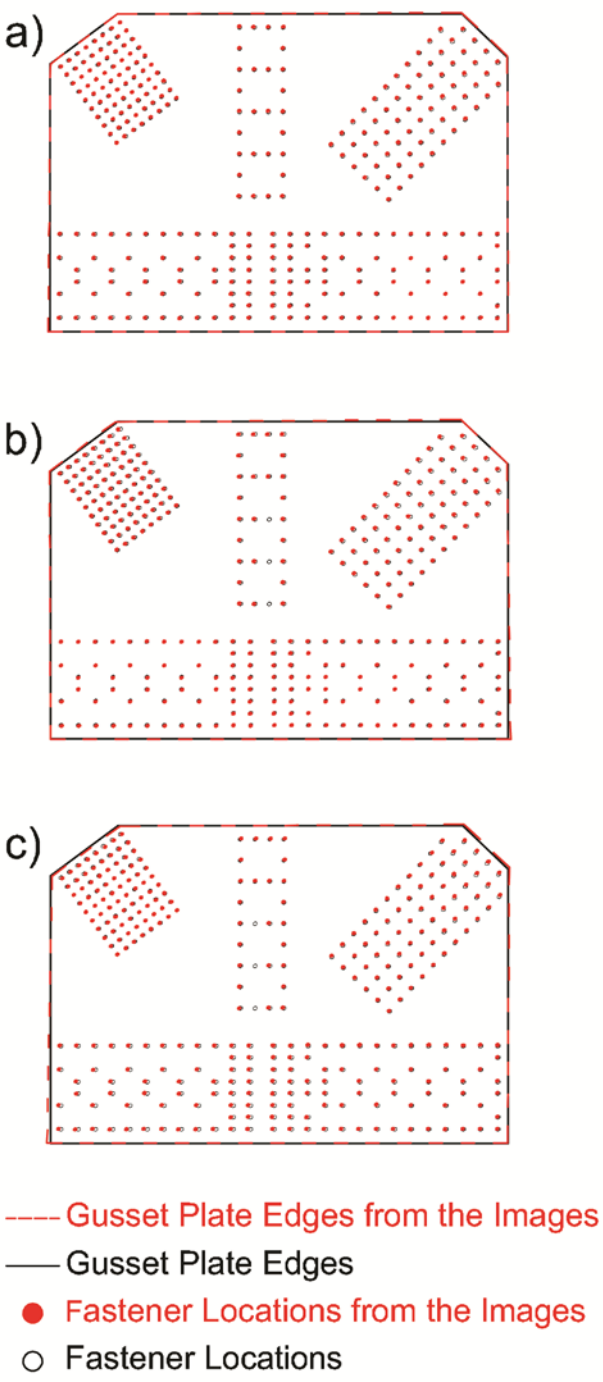

Fig. 3. Qualitative comparison of image data with CNC input file geometry for a) S90, b) S30L and c) S30R

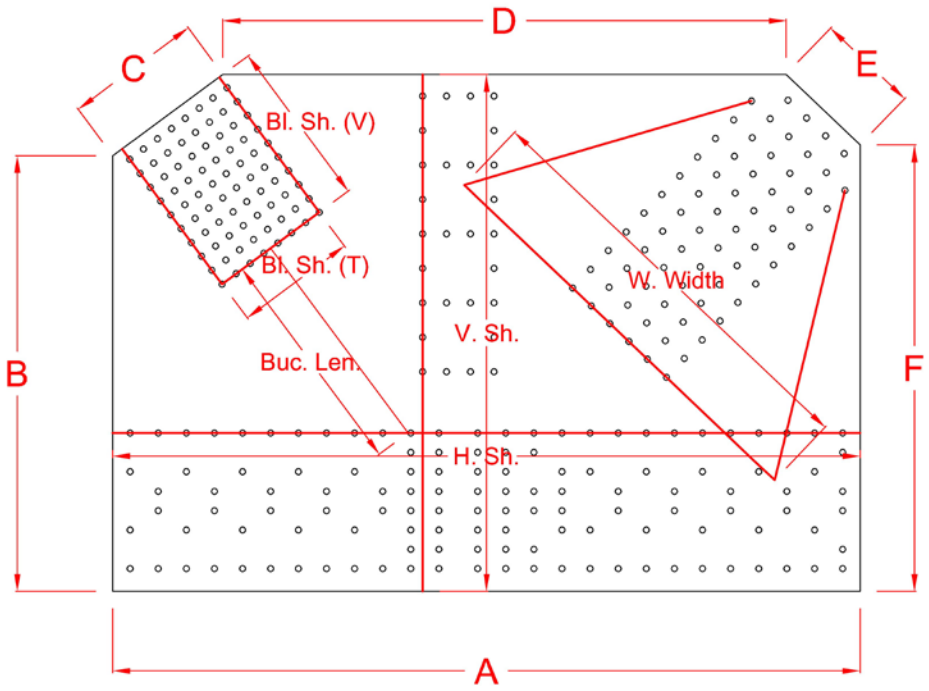

Fig. 4. Gusset plate geometric parameters used to compare the image measurement with the CNC input file geometry (for simplicity Bl. Sh. (V), Bl. Sh. (T), Buc. Len, W. Width are not shown for every member).

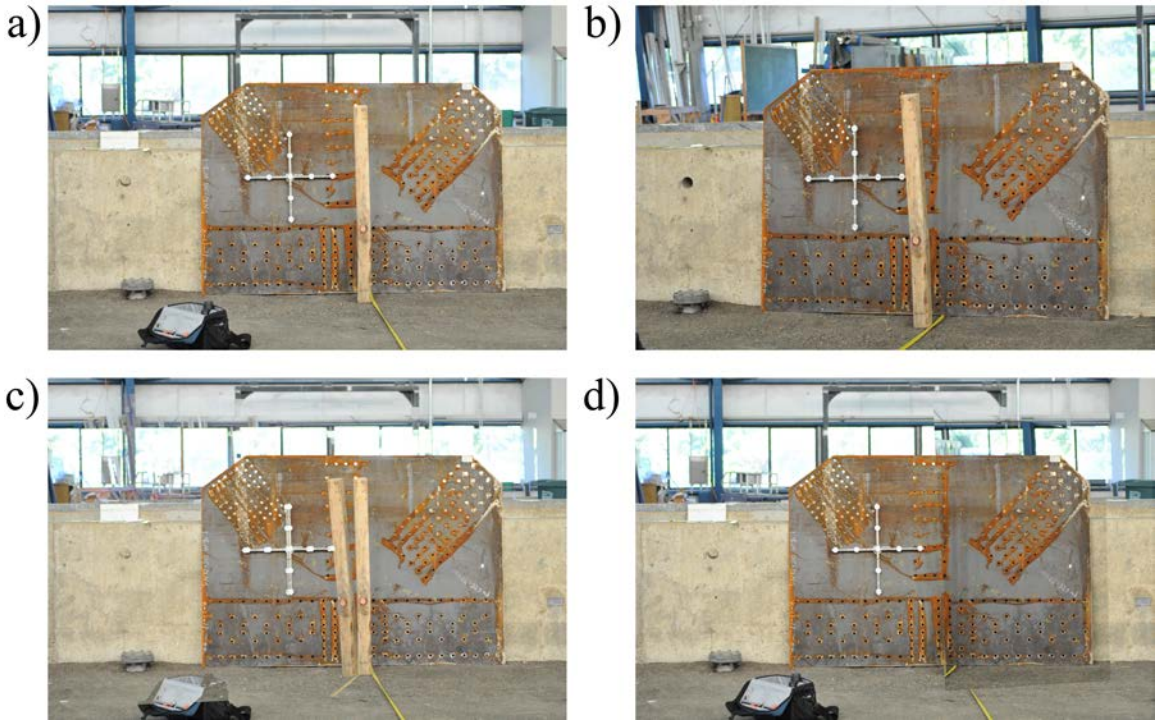

Fig 5. Demonstration of stitching two images together to make a composite image that retains geometric scale a) Image 1, b) Image 2, c) Stitched image, d) Final image

Base Region	Intersection Region	Transformed Region	
Base Image	Base Image	Black (0,0,0)	→ Base Image
Black (0,0,0)	Trans. Image	Trans. Image	→ Transformed Image
Base Image	(Base-Trans) Image	Trans. Image	→ Subtracted = Base -Transformed
Base Image	Base Image	Trans. Image	→ Stitched = Subtracted + Transformed

Fig. 6. Illustration of adding and subtracting procedure for stitching two images together.

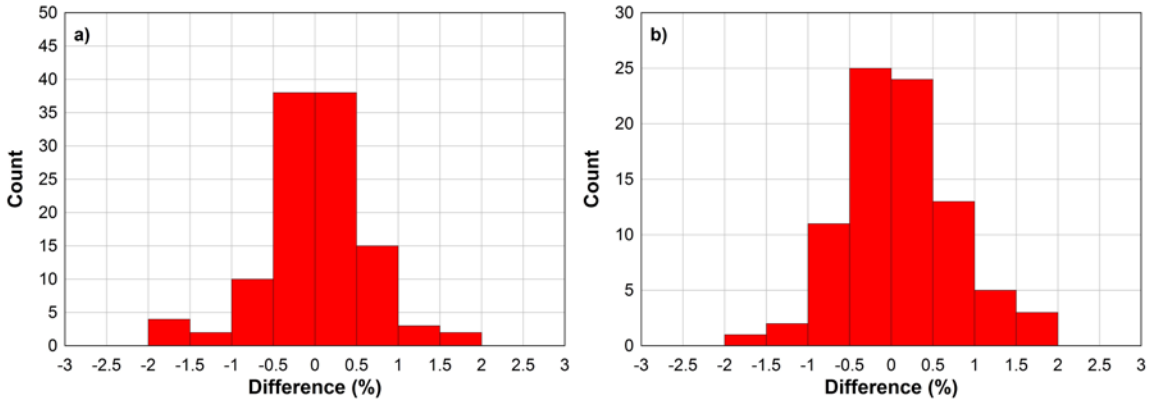

Fig 7 Histogram of differences between expected and measured values for structural parameters from a) Flat-field lens b) Fisheye Lens.

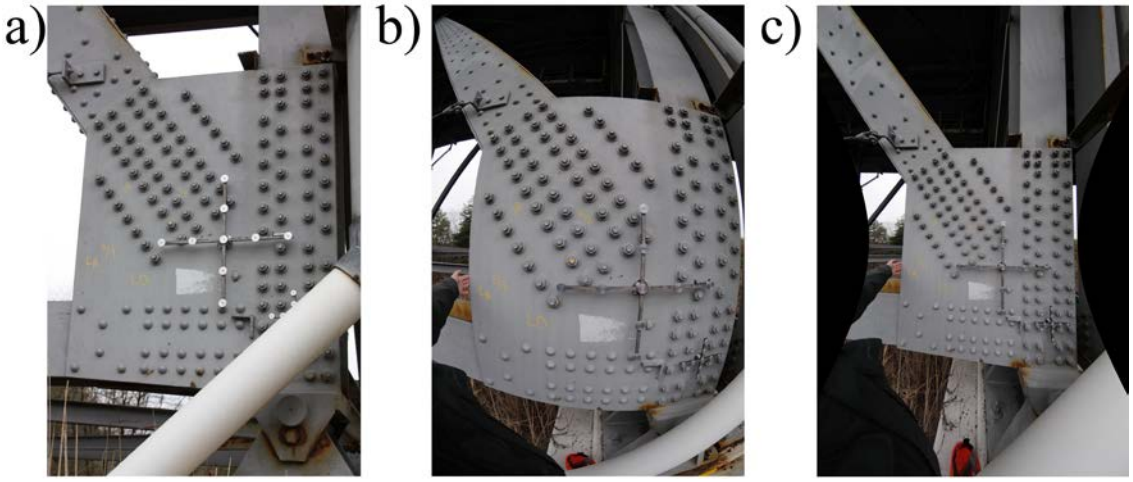

Fig.8. An image of a gusset captured by a) flat-field lens, b) fisheye lens. c) defished image. Note the downspout obstruction in the three images.

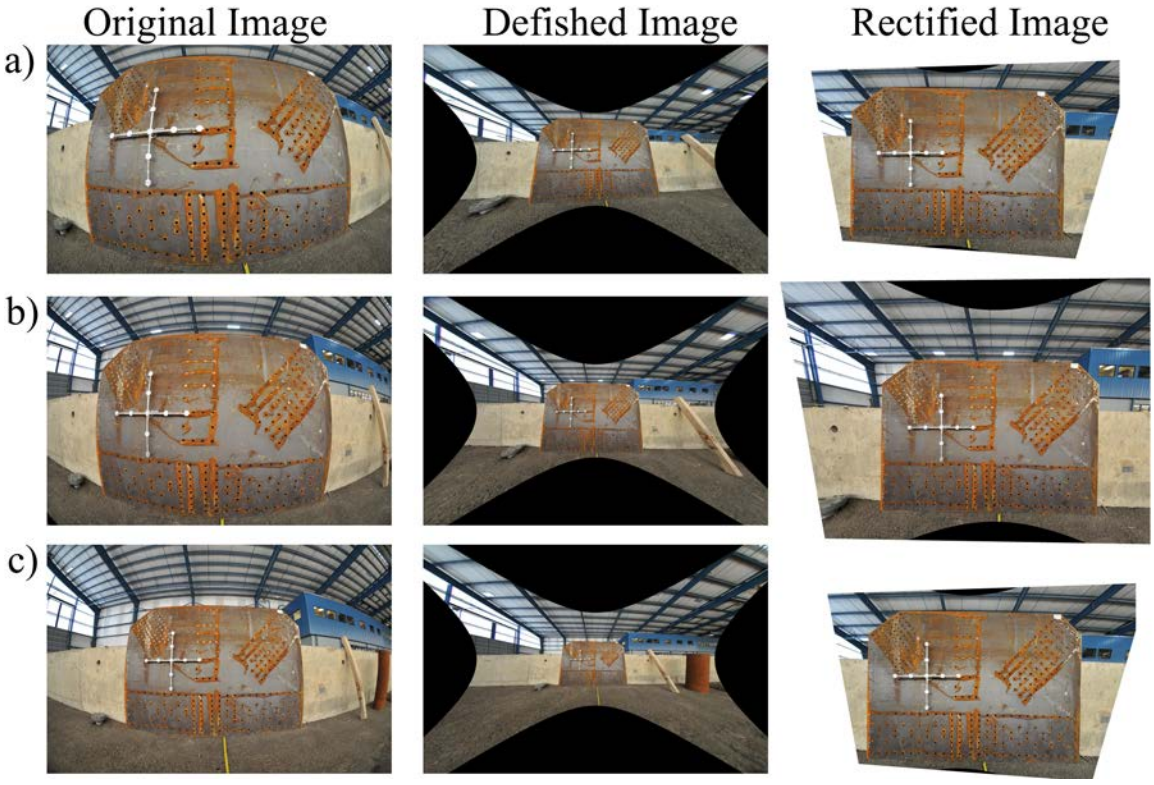

Fig.9. Original, defished, and rectified images for a) F2ft, b) F3ft and c) F5ft

Tables:

Table 1. Measurements from images taken with flat-field lens.

		L. (mm)	Flat-field lens							
			S90		S30L		S30R		Sti.	
			L. (mm)	Dif. (%)	L. (mm)	Dif. (%)	L. (mm)	Dif. (%)	L. (mm)	Dif. (%)
Member 1	Bl. Sh. (V)	958.9	952.8	-0.63	958.4	-0.05	960.2	0.14	957.5	-0.14
	Bl. Sh. (T)	466.7	466.7	-0.01	467.9	0.26	469.7	0.63	467.8	0.23
	W. Width.	991.0	988.5	-0.25	989.1	-0.20	999.2	0.83	989.9	-0.11
	Buc. Len.	114.3	114.4	0.09	112.5	-1.58	116.4	1.86	113.5	-0.73
Member 2	Bl. Sh. (V)	990.6	987.3	-0.33	991.6	0.10	976.4	-1.44	990.1	-0.05
	Bl. Sh. (T)	355.6	354.4	-0.33	355.5	-0.04	356.1	0.15	353.8	-0.50
	W. Width.	883.5	879.9	-0.41	886.2	0.31	876.2	-0.83	881.7	-0.20
	Buc. Len.	678.3	672.5	-0.86	686.2	1.17	669.5	-1.29	675.6	-0.40
Member 3	Bl. Sh. (V)	1752.6	1753.0	0.02	1754.0	0.08	1751.1	-0.09	1746.6	-0.34
	Bl. Sh. (T)	209.6	209.4	-0.09	209.3	-0.12	209.5	-0.02	210.2	0.31
	W. Len.	1148.1	1146.4	-0.15	1149.3	0.11	1148.3	0.02	1144.8	-0.29
	Buc. Len.	181.0	181.5	0.27	181.0	0.00	179.3	-0.91	179.4	-0.90
Member 4	Bl. Sh. (V)	1695.7	1711.3	0.92	1700.3	0.27	1708.1	0.73	1696.4	0.04
	Bl. Sh. (T)	381.0	380.2	-0.22	384.2	0.85	380.6	-0.11	381.4	0.12
	W. Width.	1260.9	1267.4	0.52	1264.3	0.27	1268.6	0.61	1259.5	-0.11
	Buc. Len.	409.4	409.5	0.02	409.2	-0.05	412.2	0.69	407.0	-0.58
Member 5	Bl. Sh. (V)	1124.0	1126.5	0.23	1133.0	0.80	1130.1	0.55	1123.2	-0.07
	Bl. Sh. (T)	466.7	466.8	0.02	470.0	0.69	469.6	0.62	467.5	0.17
	W. Width.	1086.3	1085.8	-0.05	1098.2	1.09	1090.6	0.40	1087.8	0.14
	Buc. Len.	114.3	114.4	0.09	112.5	-1.58	116.4	1.86	113.5	-0.73
Edge Length	A	2197.1	2193.6	-0.16	2207.2	0.46	2211.1	0.64	2194.2	-0.13
	B	1284.4	1282.2	-0.17	1285.8	0.11	1282.1	-0.18	1281.0	-0.26
	C	402.9	399.8	-0.75	395.2	-1.91	403.1	0.05	396.8	-1.51
	D	1655.6	1656.4	0.05	1657.6	0.12	1653.9	-0.10	1655.5	-0.01
	E	300.7	300.7	-0.01	304.1	1.12	298.4	-0.79	301.9	0.39
	F	1316.4	1320.8	0.33	1324.8	0.64	1323.4	0.53	1318.4	0.15
	H. Sh.	2197.1	2193.5	-0.16	2203.1	0.28	2205.0	0.36	2194.5	-0.12
	V. Sh.	1524.0	1524.0	0.00	1526.2	0.14	1524.0	0.00	1519.9	-0.27
	Abs. Max.			0.92		1.91		1.86		1.51
	Mean			-0.07		0.12		0.18		-0.21

Table 2. Measurements from images taken with fisheye lens.

		L. (mm)	Fisheye					
			F2ft		F3ft		F5ft	
			L. (mm)	Dif. (%)	L. (mm)	Dif. (%)	L. (mm)	Dif. (%)
Member 1	Bl. Sh. (V)	958.9	954.8	-0.43	953.5	-0.56	958.7	-0.01
	Bl. Sh. (T)	466.7	475.3	1.83	473.6	1.47	471.7	1.07
	W. Width.	991.0	999.4	0.85	995.3	0.43	994.5	0.35
	Buc. Len.	114.3	115.4	0.94	115.3	0.84	114.2	-0.06
Member 2	Bl. Sh. (V)	990.6	975.1	-1.57	978.5	-1.22	991.6	0.10
	Bl. Sh. (T)	355.6	356.9	0.36	356.3	0.19	356.4	0.24
	W. Width.	883.5	877.6	-0.67	877.7	-0.66	884.4	0.10
	Buc. Len.	678.3	683.6	0.79	681.0	0.40	680.5	0.33
Member 3	Bl. Sh. (V)	1752.6	1741.2	-0.65	1740.4	-0.70	1747.1	-0.31
	Bl. Sh. (T)	209.6	211.3	0.83	209.5	-0.01	210.1	0.27
	W. Len.	1148.1	1149.8	0.15	1145.6	-0.21	1146.3	-0.16
	Buc. Len.	181.0	182.0	0.54	180.8	-0.08	180.9	-0.04
Member 4	Bl. Sh. (V)	1695.7	1675.2	-1.21	1685.1	-0.63	1691.8	-0.24
	Bl. Sh. (T)	381.0	384.0	0.80	383.4	0.63	381.8	0.22
	W. Width.	1260.9	1252.6	-0.65	1257.2	-0.29	1255.9	-0.40
	Buc. Len.	409.4	410.5	0.28	410.0	0.15	409.4	0.01
Member 5	Bl. Sh. (V)	1124.0	1115.5	-0.75	1121.8	-0.19	1120.0	-0.35
	Bl. Sh. (T)	466.7	475.3	1.83	474.0	1.56	471.9	1.11
	W. Width.	1086.3	1095.8	0.88	1098.6	1.13	1092.6	0.58
	Buc. Len.	114.3	115.4	0.94	115.3	0.84	114.2	-0.06
Edge Length	A	2197.1	2182.5	-0.67	2188.2	-0.41	2189.9	-0.33
	B	1284.4	1280.9	-0.27	1278.1	-0.49	1284.0	-0.03
	C	402.9	403.9	0.25	400.4	-0.62	402.2	-0.17
	D	1655.6	1655.2	-0.03	1656.4	0.05	1660.8	0.31
	E	300.7	301.6	0.28	304.8	1.34	303.4	0.87
	F	1316.4	1317.0	0.04	1316.8	0.03	1313.4	-0.23
	H. Sh.	2197.1	2185.2	-0.54	2189.8	-0.33	2193.0	-0.19
	V. Sh.	1524.0	1527.7	0.24	1524.5	0.04	1526.4	0.16
	Abs. Max.			1.83		1.56		1.11
	Mean			0.16		0.10		0.11